J.M. Teissier[1], I.M.L. Ridge[2], J.J. Evans[2] and M. Fournier[1] **ODN 0949**
[1]DEP Engineering, Saint Martin d'Hères, France; [2]TTI Testing, Wallingford, UK

The effect of wire break distribution on the breaking strength of a wire rope

Summary

The work presented in this paper was conducted with a view to assess the effect of the distribution of wire breaks on the breaking strength of a spiral strand rope. It has been previously noted that the loss in breaking strength of a rope with wire breaks can be more than the effective loss in metallic area and this is especially true if the breaks are asymmetric. A ratio "k" has been used to characterise this where a value of 1 means that the strength loss is exactly equivalent to metallic area loss and higher values of k mean that the strength loss is (proportionally) higher than the metallic area loss.

A review has been made of previous work undertaken by Oplatka [**1**] and SIMRAC (the South African "Safety in Mines Research Advisory Committee") [**2**] for various constructions of six strand rope. The results appear to show a value of k varying from 2 - 3 for increasingly severe levels of asymmetric damage, with a value closer to 1 for symmetric damage. In addition to the earlier studies, series of tests on artificially damaged six strand ropes have been undertaken and the results of these tests appear to be broadly in agreement with the previous work.

A series of breaking tests have been made on two different constructions of wire strand with various levels of damage. An FE simulation has been developed for one construction and comparative measurements made on a strain gauged sample, undertaking load-unload tests for various levels of damage. The experimental results indicate that the k factor does not deviate significantly from 1 for all of the asymmetric configurations considered which was not as expected or predicted by the initial FE model. The strain gauge experiment provided some insight as to the reason for this behaviour. Tests on a single wire show a large level of plastic deformation before the wire fails (at 4%) and although significant asymmetric load sharing of wires is measured for lower loads, as the loads moves towards the rope break there is a convergence of wire load values which become much more evenly distributed at the point of ultimate failure. By re-running the FE model with the non-linear stress strain relationship it is possibly to partially simulate this behaviour although there is still a discrepancy, possibly caused by physical wire realignments taking place which have not been considered in the model.

It is concluded that although k is a useful parameter for six strand rope, it is not an appropriate measure for determining strength loss in an asymmetrically damaged strand. However, there will be much more significant endurance loss caused by variations in wire load in standard operation load range of the rope. The use of an amplification factor to quantify this is proposed, with the suggestion that it could be incorporated into the rope discard criteria.

1 Motivation of the study

At the OIPEEC conference in Oxford (2013) the authors presented the results of a study investigating the influence of the so called “safety” clamp on a rope termination [**3**]. The conclusion of this work was that the real effect of the “safety” clamp was a dramatic reduction of the service of the rope: for a full locked coil rope at given loading conditions the loss in endurance was as much as 80%.

About one year after this publication, for one of the examples presented in the paper (that of a cable stayed bridge) significant groups of wire breaks were found during a routine inspection (Figure 1).

This damage raised the question: what is the residual breaking strength of a rope with such damage?

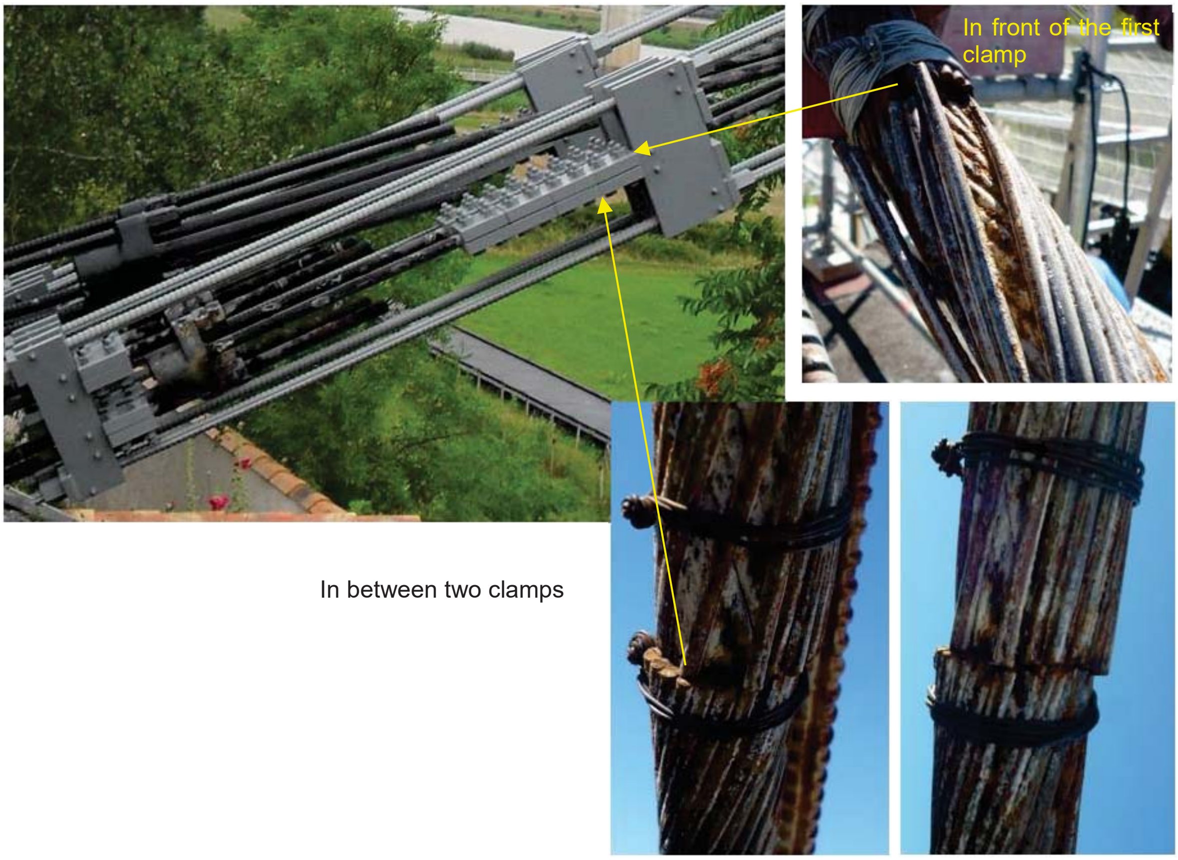

Figure 1: Wire breaks on a spiral strand rope suffered in service with a "safety" clamp. (Note that in this example a series of four safety clamps have been employed on each cable.)

2 Overview of the work

A review of literature published on the effect of wire breaks on strength of a rope identified only work undertaken on stranded ropes [**1**, **2**]. The results from these studies were assessed in order to identify possible influencing factors (such as rope diameter, stiffness, construction…). After this review, comparative breaking load tests were made on six strand ropes performed to confirm the conclusion of this analysis.

In parallel to this work, tests and calculations were also made with spiral strand rope.

However, simply measuring the remaining breaking strength of the spiral strand did not provide sufficient information to sensibly compare the results of breaking strength measurements and calculations. In order to address this problem, a sample of one of the spiral strand ropes was prepared with strain gauges on each of its outer wires.

Finally tests were performed to evaluate whether the same factor of influence identified for the stranded rope also applied to the spiral strand rope.

3 Evaluation of the influence of the wire break distribution

3.1 Parameters for this study

The following parameters were defined in this work:

A_0	= Initial metallic section (mm²)
A	= Residual metallic section (mm²)
F_0	= Initial breaking strength (kN)
F	= Residual breaking strength (kN)
$(A_0 - A)/A_0 = 1-A/A_0$	= Loss of metal section (%)
$(F_0 - F)/F_0 = 1-F/F_0$	= Loss of strength (%)

The factor **k** is the ratio between the loss of strength and the loss of metallic section:

$$(F_0 - F)/F_0 = k \times [(A_0 - A)/A_0]$$

$$k = (1 - F/F_0)/(1 - A/A_0)$$

3.2 Definition of the degree of asymmetry

The asymmetry of the damage must be taken into account with respect to both the X axis and the Y axis.

The position and the number of cut wires are identified using a similar notation to that employed in the SIMRAC paper, and as shown in Figure 2.

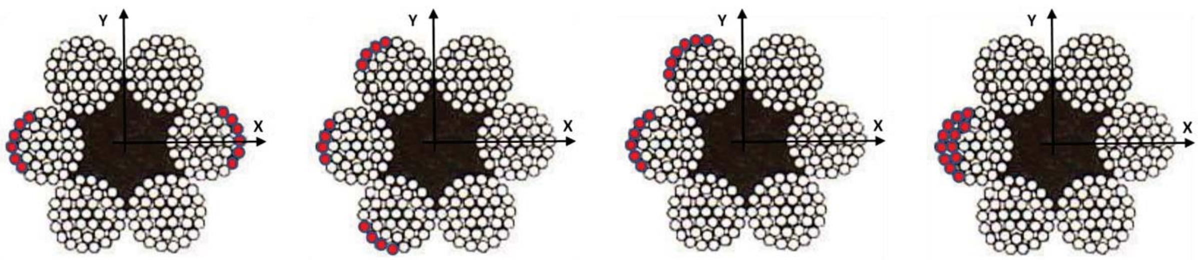

Symmetry	Partial symmetry	Partial symmetry	Asymmetry
6.0.0 0.0.6	4.4.4 0.0.0	6.6.0 0.0.0	12.0.0 0.0.0

Figure 2: Notation used to define the degree of asymmetry.

4 Analysis of the existing work

4.1 Results from Prof. Oplatka

Professor Oplatka tested mainly symmetrical or almost symmetrical configurations. The tests were performed on Ø22.5 mm ropes with constructions 6×7 + FC and 6×17 + FC both Lang's and ordinary lay. The most asymmetrical configurations tested were in tests I/5 and I/18 (Table 1).

It is noted that for all the tests the loss of metallic area was significant (from 32% to 84%), well beyond the discard criteria for the rope.

Rope	Test no.	A/A_0 [%]	F/F_0 [%]	Type of symmetry	k
6×(1+6)+FC / L	I/1	52	45	3.3.3 3.3.3 (int.)	1.15
6×(1+6)+FC / L	I/2	52	47	3.3.3 3.3.3 (ext.)	1.10
6×(1+6)+FC / L	I/3	52	48	3.3.3 3.3.3 (mix.)	1.08
6×(1+6)+FC / L	I/4	52	54	3.3.3 3.3.3 (mix.)	0.96
6×(1+6)+FC / L	I/5	52	28	5.5.5 3.0.0	1.50
6×(1+6)+FC / L	I/6	36	22	5.5.5 5.2.2 (int.)	1.22
6×(1+6)+FC / L	I/7	36	24	5.5.5 5.2.2 (int.)	1.19
6×(1+6)+FC / L	I/8	36	22	5.5.5 5.2.2 (int.)	1.22
6×(1+6)+FC / L	I/9	36	23	5.5.5 5.2.2 (mix.)	1.20
6×(1+6)+FC / L	I/10	36	23	4.4.4 4.4.4	1.06
6×(1+6)+FC / L	I/11	28	18	5.5.5 5.5.2 (int.)	1.14
6×(1+6)+FC / L	I/12	28	18	5.5.5 5.5.2 (ext.)	1.14
6×(1+6)+FC / L	I/13	20	21	5.5.5 5.5.5 (ext.)	0.99
6×(1+6)+FC / L	I/14	20	20	5.5.5 5.5.5 (int.)	1.00
6×(1+6)+FC / L	I/15	20	15	5.5.5 5.5.5 (mix.)	1.06
6×(1+6)+FC / L	I/16	16	13	6.6.6 6.6.6 (mix.)	1.04
6×(1+6)+FC / L	I/17	25	18	2.2.2 2.2.2 (ext.)	1.09
6×(1+6)+FC / L	I/18	68	51	4.4.4 0.0.0	1.53
6×(1+6)+FC / L	II/1	43	30	5.5.5 5.2.2 (int.)	1.23
6×(1+6)+FC / R	III/1	43	34	5.5.5 5.2.2 (int.)	1.16
6×(1+8+8)+FC / L	IV/1	28	19	7.7.7 7.5.5 (mix.)	1.13
6×(1+8+8)+FC / R	V/1	28	23	7.7.7 7.5.5 (mix.)	1.07
6×(1+8+8)+FC / R	V/2	28	28	6.6.7 6.6.7 (int.)	1.00

Table 1: Summary of the results of the tests reported by Prof. Oplatka [**1**] (L = Lang's lay, R = regular or ordinary lay).

4.2 Results from SIMRAC

A significant number of tests were performed on ropes of different diameters (Table 2). Most of the ropes were triangular strand with a fibre core, as this construction was applicable to the mine hoisting application of interest to the research committee. Each sample was prepared by casting white metal sockets before cycling 500 times between 5% and 25% of the new rope breaking strength before cutting the desired numbers of wires. Comparative tests were also conducted on a Ø41 mm rope with the cycling conducted after the wires had been cut, or with no cycling at all.

Tests carried out by Borello and Kuun in 1994 [**2**] investigated different kinds of symmetry. Later tests performed by Hecker and Kuun in 1996 [**2**] were limited to asymmetrical wire break configurations (N.0.0 0.0.0).

Triangular Strand Rope	**Diameter [mm]**	**Number of tests**	
6 × 32 + FC	48	46	Borello and Kuun, 1994
6 × 36 + FC	63	3	
6 × 34 + FC (new)	62	5	Hecker and Kuun, 1996
6 × 34 + FC (discarded)	62	20	
6 × 32 + FC	48	11	
6 × 26 + FC	32	7	
6 × 29 + FC	41	22	
Round Strand Rope			
6 × 25 + IWRC	48	5	
		119	

Table 2: Overview of the tests performed by SIMRAC [**2**].

4.3 Analysis of the SIMRAC results

4.3.1 Scatter among the results

Each configuration of cut wires was tested several times, from two to six times.

The following graph (Figure 3) summarises the results of the Triangular Strand ropes for the asymmetric configuration (N.0.0 0.0.0).

It may be seen that there is significant scatter among these results. For the same rope, for the same diameter and for the same cut wire configuration variations of the k factor of 20% to 45% are apparent.

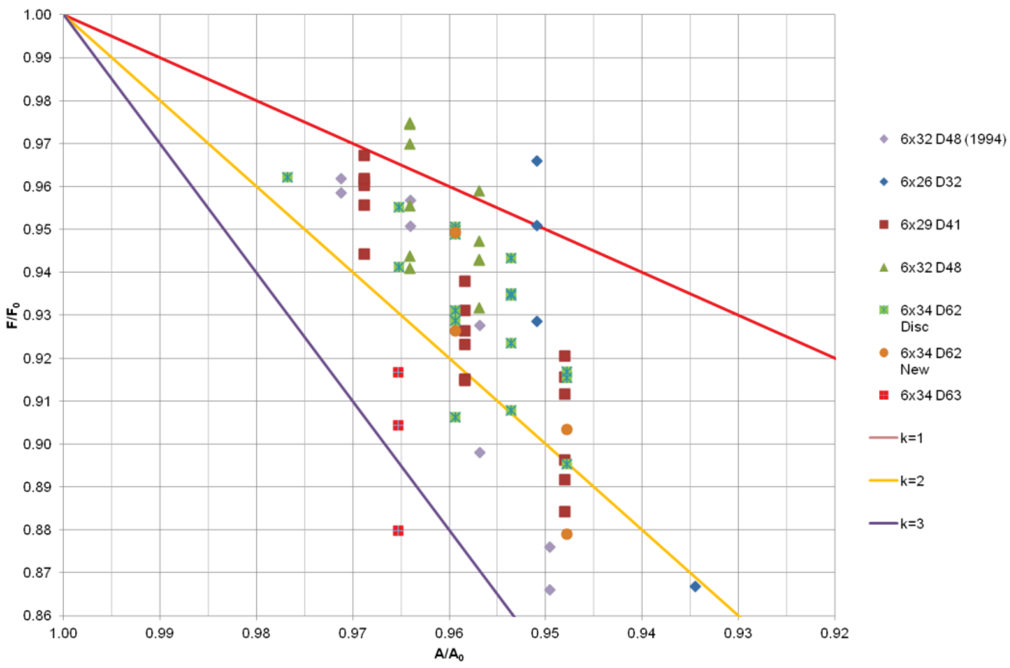

Figure 3: SIMRAC - Results for asymmetric configuration – Scatter.

4.3.2 Influence of the diameter

To accommodate the scatter noted above, the average result for each test configuration has been used.

The following graph (Figure 4) shows the results of the Triangular Strand ropes for the asymmetric configuration (N.0.0 0.0.0).

It is obviously impossible to establish a rule that indicates how the diameter of the rope influences the k factor.

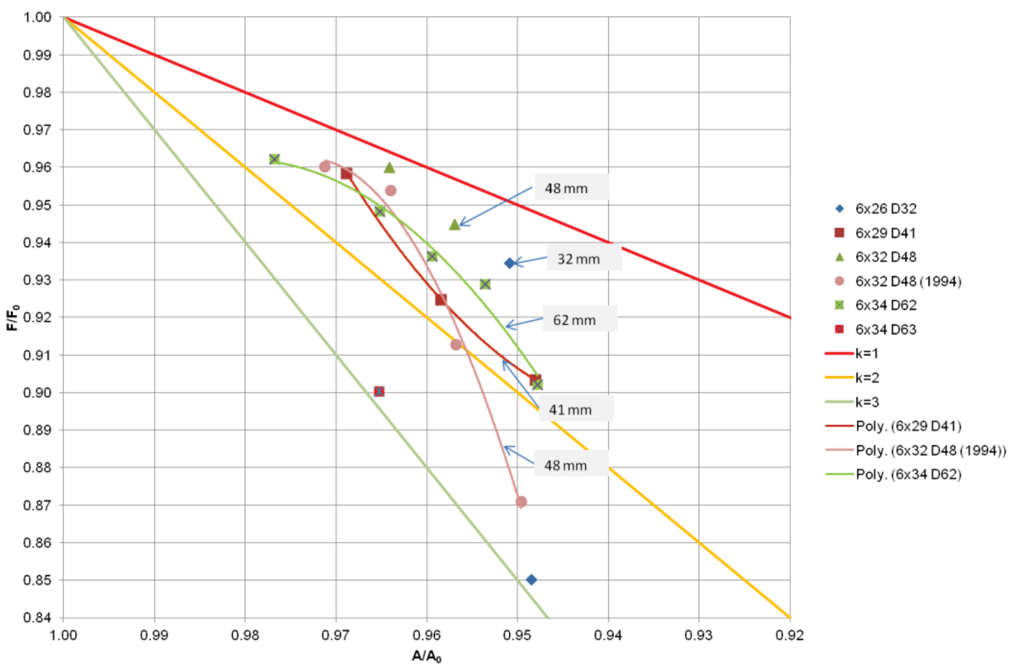

Figure 4: SIMRAC - Asymmetric configuration – Influence of the rope diameter.

4.3.3 Influence of the stiffness

Figure 5 compares the behaviour of a Round Strand with IWRC to the behaviour of a Triangular Strand rope with Fibre Core. Only ropes of 48 mm diameter have been taken into account.

The Round Strand rope with IWRC is stiffer than the Triangular Strand rope with fibre core.

There are only a few measurements available for the rope with IWRC, but it seems that the k factor decreases slightly if the rope gets stiffer, which does not seem logical. The difference is, however, not significant if we take into account the discrepancies identified above.

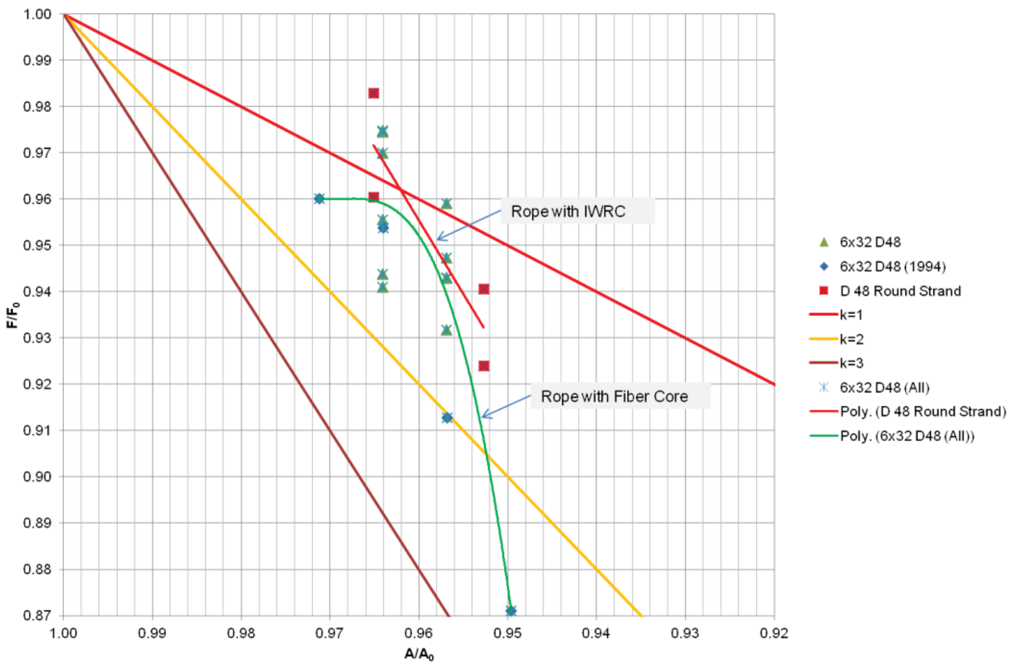

Figure 5: SIMRAC - Asymmetric configuration – Influence of the rope stiffness.

4.3.4 Influence of the degree of asymmetry

In order to assess the influence of the degree of asymmetry, the following configurations: (N.0.0 0.0.0), (N.N.0 0.0.0) and (N.N.N 0.0.0) have been considered (tests performed by Borello and Kuun, 1994). The tests performed by Hecker and Kuun, 1996 are related to the configuration (N.0.0 0.0.0).

Figure 6 presents a summary of the results for all these tests.

For the configuration (N.N.N 0.0.0) only two SIMRAC results were available.

The tests performed by Oplatka, (5.5.5 3.0.0) and (4.4.4 0.0.0) are quite close to the configuration (N.N.N 0.0.0). However, the results are not visible on the graph because the loss of metallic area is much bigger than that of the SIMRAC tests.

However, the fitted curve for the (N.N.N 0.0.0) includes the SIMRAC results and the Oplatka results.

The degree of asymmetry significantly influences the results. The **k** factor increases when the degree of asymmetry increases.

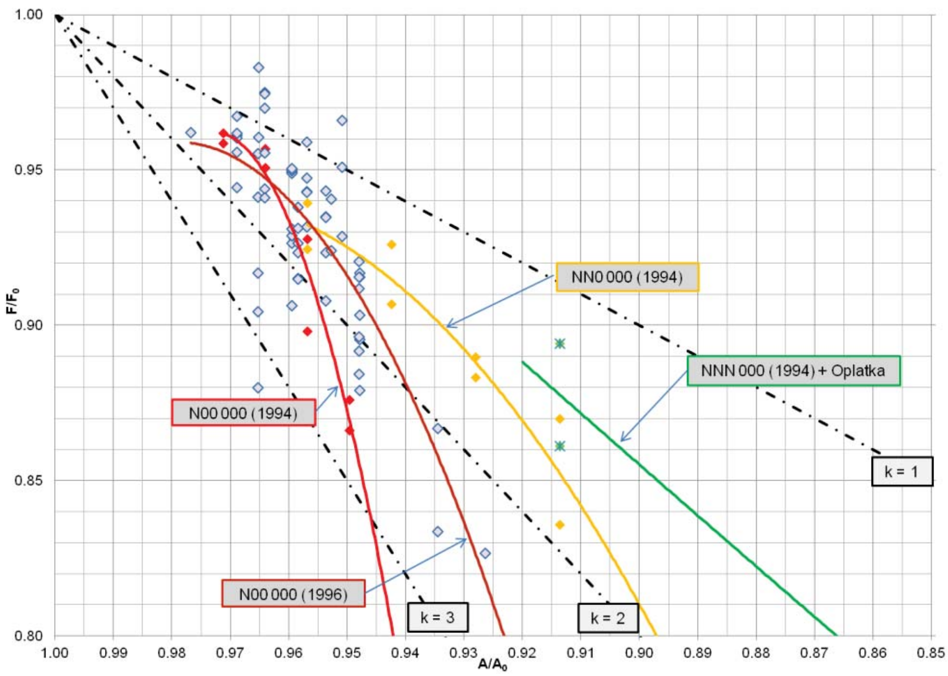

Figure 6: SIMRAC - Asymmetric configuration – Influence of the degree of asymmetry.

5 Test samples

Table 3 summarises the stranded ropes and spiral strand which were used in this study.

Cross section	Construction details
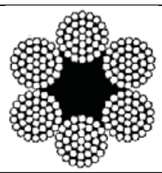	Ø16 mm and Ø28 mm 6×37 (1-6/12/18) - FC sZ Ø16 mm 1960 N/mm² grade, MBL 148 kN Ø28 mm 1770 N/mm² grade, MBL 408 kN
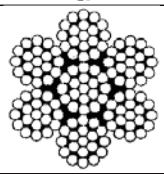	Ø16 mm 6×19 (1-6/12) - WSC 1960 N/mm² grade, MBL 182 kN
	Ø16 mm 1 × 19 (1-6/12) sZ, galv. Class A 1770 N/mm² grade, MBL 246.4 kN
	Ø16 mm 1 × 37 (1-6/12/18) 1570 N/mm² grade, MBL 230 kN

Table 3: Details of the ropes used in the study.

6 Testing equipment

TTI Testing has a number of machines suitable for the tensile testing of ropes. Two machines were used in programme of work, the 600 kN machine, which is a long horizontal machine (Figure 7), and the 250 kN vertical 'Dartec'.

Table 4 lists the main parameters of these two pieces of equipment.

Figure 7: 600 kN testing machine at TTI Testing's laboratory in Wallingford, UK.

Parameter		
Load capacity (kN)	600	250
Actuator stroke (mm)	2,000	150
Adjustable cross head for slack removal	Y	Y
Moveable 'static' crosshead	Y	N/A
Bed length (mm)	13,000	1,250
Controller	Cube SERIES	Cube SERIES
Fatigue rated	Y	Y
Block loading	Y	Y
Service (random) loading (waveform from .xls file)	Y	Y

Table 4: Main parameters of the 600 kN long bed and 'Dartec' tensile testing machines.

7 Breaking test results with stranded ropes

Initial tests were conducted on the stranded ropes. Samples were terminated using Wirelock® resin compound, the wires were cut and the rope cycled five times to 50% rope MBL before breaking. The results for these tests on the three different stranded ropes are presented in Tables 5, 6 and 7.

Cut wires	%CSA cut	Comments	Breaking Load	% CSA residual	% residual strength	k
[-]	[%]	[-]	[kN]	[%]	[%]	[-]
0	0	**(0.0.0 0.0.0)**	184.8	100	100	1.00
4	2.8	**(4.0.0 0.0.0)**	181.8	97.2	98.4	0.57

Table 5: Cut wire tests on Ø16 mm Six strand rope with WSC (7 × 19).

Cut wires	%CSA cut	Comments	Breaking Load	% CSA residual	% residual strength	k
[-]	[%]	[-]	[kN]	[%]	[%]	[-]
0	0	**(0.0.0 0.0.0)**	174.5	100	100	1.00
4	1.8	**(4.0.0 0.0.0)**	171.2	98.2	98.1	1.06

Table 6: Cut wire tests on Ø16 mm Six strand rope with FC (6 × 36 + FC).

Cut wires	%CSA cut	Comments	Breaking Load	% CSA residual	% residual strength	k
[-]	[%]	[-]	[kN]	[%]	[%]	[-]
0	0	**(0.0.0 0.0.0)**	521.7	100	100	1.00
4	1.8	**(4.0.0 0.0.0)**	508.5	98.2	97.5	1.39
8	3.6	**(8.0.0 0.0.0)**	485.2	96.4	93.0	1.94
16	7.2	**(8.8.0 0.0.0)**	469.0	92.8	89.9	1.40
24	10.7	**(8.8.8 0.0.0)**	456.2	89.3	87.4	1.17
24	10.7	**(4.4.4 4.4.4)**	470.2	89.3	90.1	0.93
12	5.3	**((8+4).0.0 0.0.0)**	449.1	94.7	86.1	2.63
24	10.5	**((8+4).(8+4).0 0.0.0)**	405.1	89.5	77.6	2.13

Table 7: Cut wire tests on Ø28 mm Six strand rope with FC (6 × 36 + FC).

Figure 8 superimposes the results of the 28 mm rope tests on those obtained by SIMRAC (Figure 6).

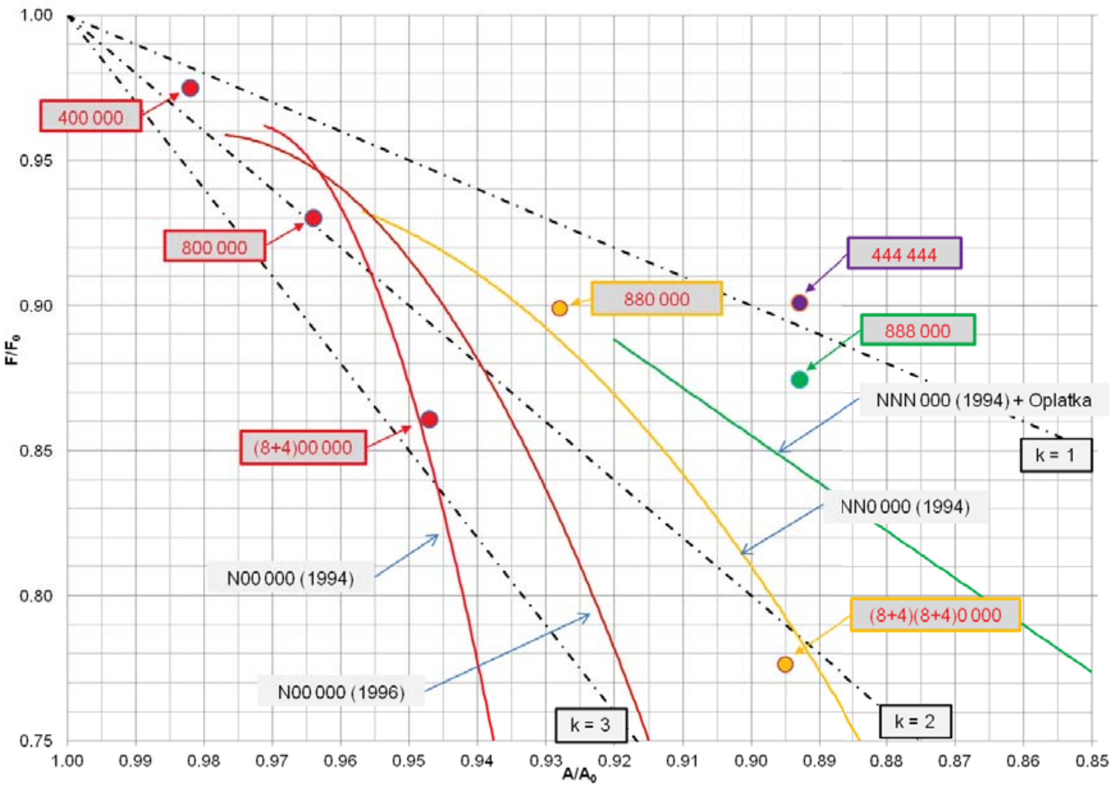

Figure 8: Results of the tests performed with the 28 mm rope.

For the configurations (N.0.0 0.0.0), the red points and for the configuration (N.N.0 0.0.0), the yellow points, the results of the tests reported here on a 6×36 + FC rope are fully in agreement with the SIMRAC results.

For the configuration (N.N.N 0.0.0), the green point, there is some discrepancy but it is noted that the green curve is based only on a few data, and furthermore that these data are obtained from different sources.

For the symmetric configuration (N.N.N N.N.N), the violet point, the **k** factor is slightly smaller than 1, which is also in agreement with the SIMRAC results.

8 Calculation of a spiral strand rope

Following review of the literature and some testing on stranded ropes, which helped to identify the critical parameters, attention was turned to model the spiral strand rope. The wires were modelled using tetragonal section 3D elements in order to facilitate the calculation of the contact between layers. Each tetragonal section had the same area as the cylindrical section of the wire. Calculations were performed using ANSYS Software Release 16.2.

	Diameter [mm]	Section [mm²]
Core	3.470	9.457
Layer 1	3.165	7.868
Layer 2	3.170	7.892

Table 8: Composition of the Spiral Strand rope.

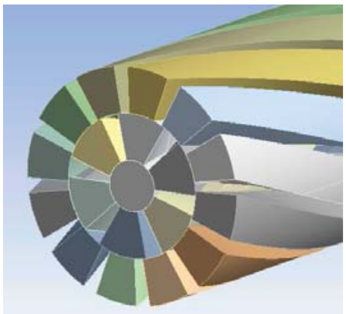

Figure 9: 3D model of the rope.

Each end of the rope was fixed, only the translation of one of them was allowed. The tensile force was applied to the end which was free to move. The cut wires were removed from the model.

To simplify the calculation model, layer one and the core wire were modelled by a single cylinder with an adapted Young's modulus.

The distribution of the forces and of the stresses in layer 2 was checked and was the same in the simplified model as with the detailed model which included all the wires.

Calculations were performed for the configurations listed in Table 9.

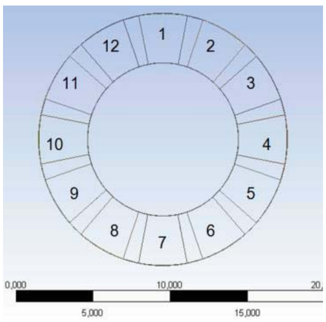

Configuration	Cut wires	Breaking load [kN]	k factor
No cut wire	-	250	1.00
2 cut wires symmetric	1 + 7	225	0.95
4 cut wires symmetric	(1 + 2) + (7 + 8)	200	0.96
8 cut wires symmetric	(1 to 4) + (7 to 10)	145	1.01
1 cut wires asymmetric	1	225	1.92
2 cut wires asymmetric	1 + 2	200	1.92
4 cut wires asymmetric	1 to 4	165	1.63
8 cut wires asymmetric	1 to 8	110	1.34

Table 9: Results of the Finite Element calculations.

With reference for Table 9, it may be seen that, as was measured with the stranded ropes, the k factor increases correspondingly with the intensity of the asymmetry.

Note that one full lay length of strand was modelled, but that in the following, the pictures show only half a lay length to aid clarity.

Once the model had been developed, attention was focused on the asymmetric configuration with 4 cut wires, because this configuration was tested with strain gauges installed on the wires (Figures 10 and 11).

The initial calculations were performed on the basis of a bi-linear stress strain curve for the wire (Figure 12).

The wires adjacent to the cut wires are the most loaded whereas the opposite wires are almost unloaded.

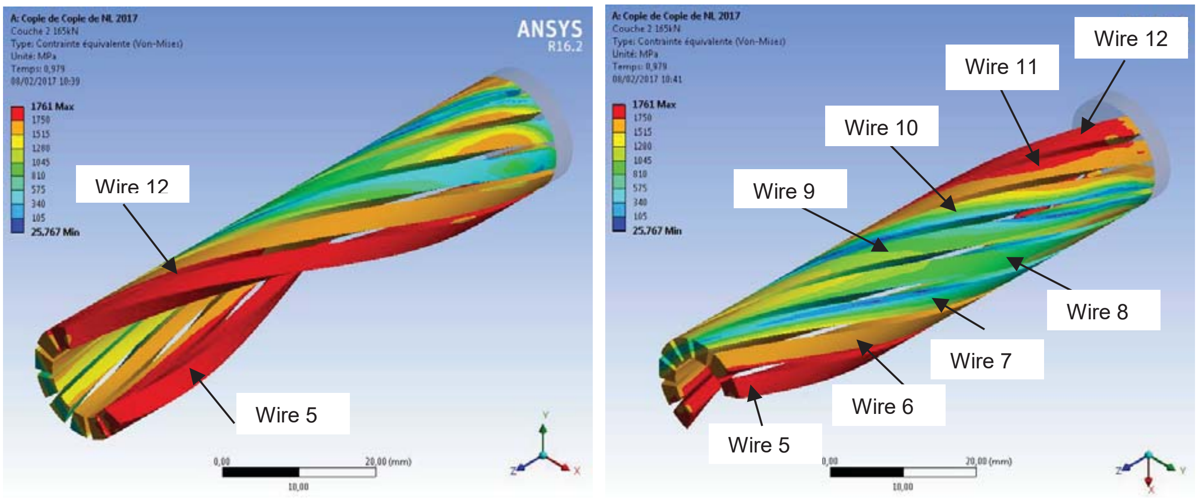

Figure 10: Distribution of the stresses among the remaining wires (cut wires n°1 - 4).

It was specified that the breaking load of the rope was attained when most of the section of the most loaded wires had reached the breaking strength of the wire. The pictures below (Figure 11) show the results of the determination of the rope's breaking strength for the configuration of '4 cut wires asymmetric'.

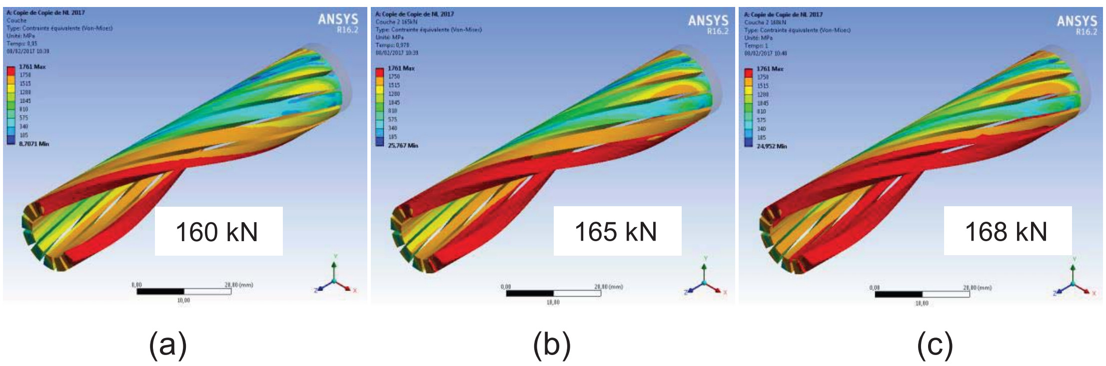

Figure 11: Evaluation of the breaking strength of the rope. (a) Shows the stress distribution for a line pull of 160 kN, the wires n°5 and n°12 have not fully reached their breaking stress, (b) for a line pull of 165 kN the whole section of these wires have reached this stress and (c) for a line pull of 168 kN, the wires n°6 and n°11 begin to reach this stress.

The results of the strain gauge measurements on a single wire (see § 9.2) made it possible to refine the model and input a more accurate stress strain curve into the software (Figure 12).

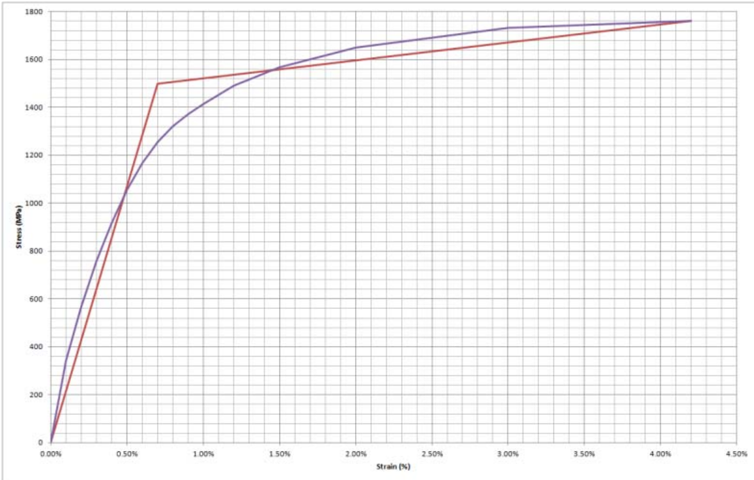

Figure 12: Bi-linear (red) stress strain curve and non linear (blue) curve.

Calculations for the asymmetric configuration with 4 cut wires were then re-run with the non-linear stress strain curve. Figure 13 presents the results of these calculations. It shows the maximum stresses in each wire (see e.g. Figure 24).

Results for wires 9 to 12 are not shown, as owing to the symmetry they are nearly identical to those of wires 5 to 8.

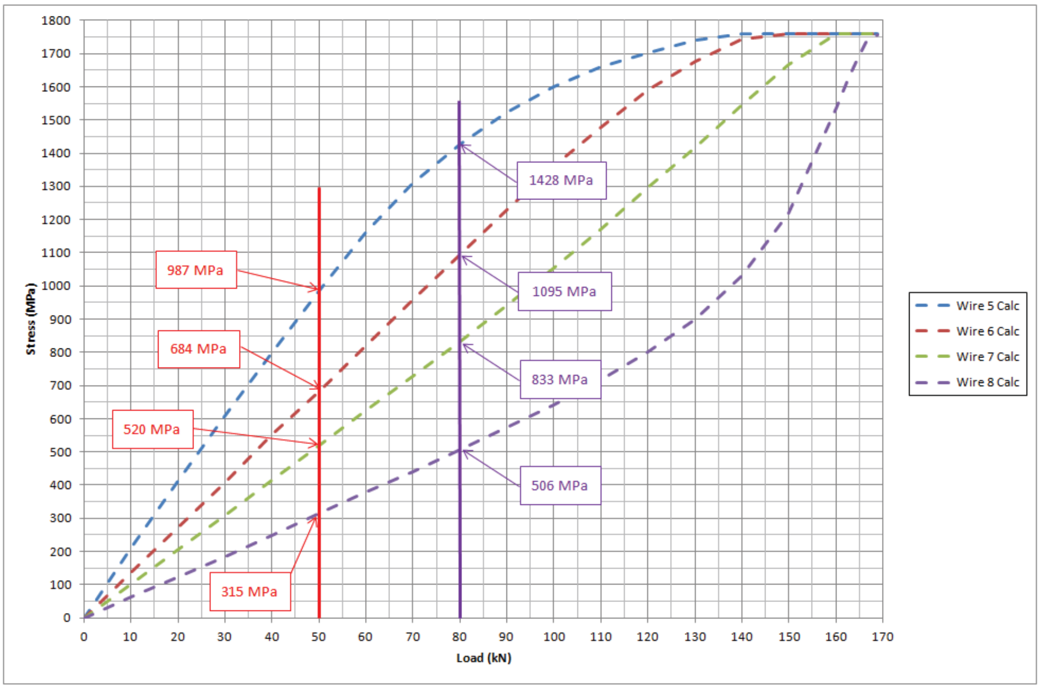

Figure 13: Results of the calculations with the non linear stress strain curve.

Owing to the flattening of the curves for the high loads, the *amplification* factor is not the same for the whole range of loading.

The amplification factor is defined as the ratio between the stress calculated with the ANSYS model and the stress for the symmetric configuration with the same number of cut wires (force divided by the remaining metallic area of the rope).

	50 kN	**80 kN**	**170 kN**
ANSYS results [MPa]	987	1428	1760
Symmetric configuration [MPa]	417	668	1419
Amplification factor	2.37	2.14	1.24
k factor	-	-	1.53

Table 10: Amplification factor versus load. 50 kN corresponds to a safety factor of 5 for a new rope, 80 kN corresponds to a safety factor of 3 for a new rope and 170 kN corresponds to the breaking strength of rope with 4 cut wires. (Note that The K factor is calculated on the basis of a breaking strength, thus there is no value for 50 kN and 80 kN).

With reference to Table 10, it may be seen that the amplification factor decreases when the loading increases.

Thus the phenomenon of amplification is more important for a rope in operation (safety factor of 5 – running rope, or safety factor of 3 – guy rope) than for a rope that is loaded almost at its breaking strength.

It is noted that the breaking strength evaluated above (170 kN) is very close to that evaluated on the basis of the calculation with bi-linear stress strain curve (165 kN – Table 9).

The amplification factor identified above (Table 10) is related to the same phenomena as the k factor (see §3), but it is calculated on the basis of the stresses whereas the k factor is calculated in the basis of the load. The k factor corresponding to a breaking load of 170 kN is 1.53 whereas the amplification factor is only 1.24 for the same load.

9 Strain gauge measurements on a spiral strand rope

In order to validate the computer model of the distribution of load between the wires in a spiral strand rope (both with and without cut wires) it was decided to undertake a series of tests with strain gauges fitted on the outer layer of wires of a sample. A length of the 1 × 19 spiral strand was used for this test, which had 12 outer wires each Ø3.17 mm.

- As a first step, a single outer wire was removed from a length of spiral strand, carefully straightened, and a single gauge applied mid length. This provided basic load-strain information for the wires in the rope.
- Following on from this, the spiral strand sample was made up and tested as described below.

9.1 Strain gauge equipment

The strain gauges used in the work reported here were standard gauges with a nominal resistance of 120 Ω and gauge factor of 2 (EA-06-031DE120 manufactured by Micro Measurements). The gauges were 0.79 mm long and 0.81 mm wide, mounted on 7 mm × 3 mm flexible backing. Gauges were attached to the wires following the recommended procedures from the manufacturer.

Each gauge was in a quarter Wheatstone bridge configuration using a Vishay 5100B multiple channel amplifier / signal conditioner controlled through a PCMCIA port by a laptop running Strainsmart software. The gauges were wired using the three wire configuration to prevent drift in readings caused by temperature variations. Calibration of the strain gauges was achieved using the shunt calibration facility in this device.

The multiple channel amplifier also had a high voltage input card which accepted the analogue signal for the actuator displacement and load from the tensile test machine. This allowed simultaneous acquisition of load, actuator displacement and strain readings which could then be exported to Excel or Matlab for further analysis.

9.2 Wire test

In order to calculate the stress in the rope wires, the stress-strain relationship was measured by testing a single wire. The wire was prepared with a strain gauge in the centre, and then tested to failure in TTI Testing's universal testing machine (Figure 14).

The stress-strain relationship was measured using both the strain gauge and also derived from the machine actuator movement. The results are presented in Figure 15 (a). In both cases the stress is calculated as the load divided by the wire cross sectional area. The strain derived from the actuator movement was calculated as the change in length divided by the initial sample length (433 mm).

It may be seen that the strain gauge derived behaviour does not show the complete break load test since the gauge failed before the wire broke. It also noted that the actuator derived strain is significantly higher than that measured by the strain gauge. The reason for this error is the effect/movement of the wedge grips which held the ends of the wire. If the Youngs' modulus (E) is derived by performing a linear fit of the first 0.5% strain of the strain gauge curve it gives a value of 204 GPa which is as expected.

To derive the stress/strain behaviour for the wire right up to the point of failure, it was necessary to 'extend' the experimentally derived strain gauge curve. To do this, the actuator and the strain gauge stress-strain values were compared (Figures 15 (b) and (c)), and the relationship shown by the dashed line in Figure 15 (a) inferred. This gives an approximate failure strain of 4% which is typical for rope wire.

This relationship was then used to derive the individual wire stress from the strain gauge results obtained in the rope tests. It is noted that this new extended non linear stress strain relationship (15^{th} order polynomial using the least square method) is only valid between 0 and 4% strain.

One consideration with this approach is that if a wire goes into a 'plastic' region during loading then this will change the stress strain behaviour if it is unloaded and reloaded. While this clearly will happen when the rope is taken to break it was thought to be a reasonable assumption to discount this for the initial 'non break' tests since each condition was tested twice and appeared to give repeatable results.

Figure 14: Wire test in universal testing machine, right, detail showing the wedged end grips.

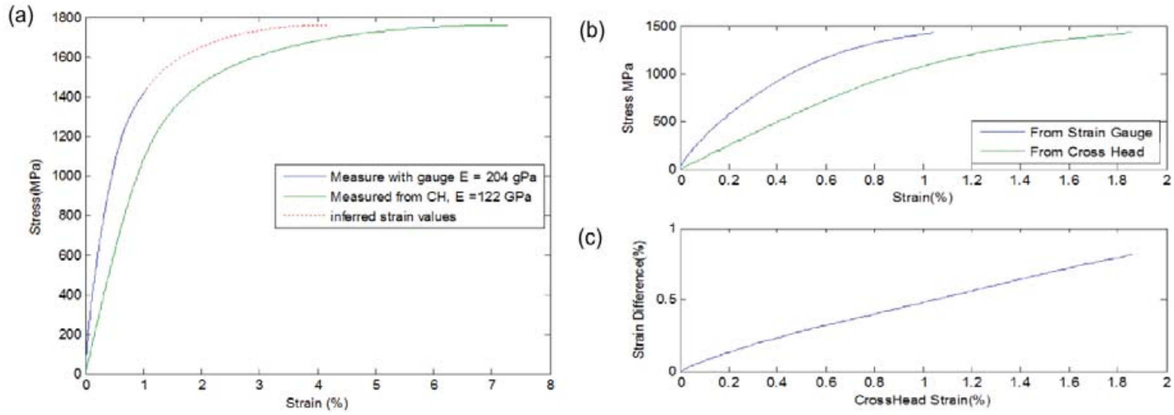

Figure 15: (a) Shows the strain gauge and the cross head derived stress-strain plot (b) Shows the results up to the gauge failure and (c) Shows the difference between the two results- if this linear relationship is extended it is possible to infer the strain gauge results up to the wire failure (shown in dashed in (a)).

9.3 Spiral strand test

A spiral strand sample (nominal length 800 mm) was terminated in TTI Testing conical sockets and completed with Wirelock® resin compound. Twelve strain gauges were mounted at the centre cross section of the sample, one gauge on each of the outer wires.

The strain gauges (numbered sequentially around the circumference 1-12, as per Table 9) were used to measure the strain in the rope under various conditions:

(1) The undamaged rope cycled up to a load of 175 kN and then unloaded;

(2) Wire 1 cut, the sample loaded to 160 kN and then unloaded;

(3) Wires 1 and 2 cut, the sample loaded to 140 kN and unloaded;

(4) Wires 1, 2, 3 and 4 loaded to 100 kN and unloaded; and finally,

(5) Rope taken to break load.

It was not practical to cut the wires at same cross section as the strain gauges owing to concerns about damaging the neighbouring gauges. Thus wires were cut 75 mm from the strain gauge position.

Each test (with the exception of the break test) was repeated at least once and the results were found to be repeatable. The strain vs. load plots for the first four cases listed above are shown in Figure 16 and the stress vs. load are shown in Figure 17. It seems clear from these results that the wires adjacent to the breaks take the highest load and the load then drops off to a minimum for the wires furthest from (opposite) the break (or breaks). It may also be seen that owing to frictional effects, there is a measurable load carried in the broken wire just a short distance from the break site. The rope break test (Figure 18) shows a convergence of wire stresses as the rope gets closer to break presumably caused by a combination of wire yielding and realignment. This kind of behaviour has been seen in past experimental work on ropes [**4**] and can give a significant increase in rope endurance. To illustrate the stress distribution more clearly the stress at 100 kN has been plotted against wire number for the undamaged rope and the three cut wire configurations (Figure 19).

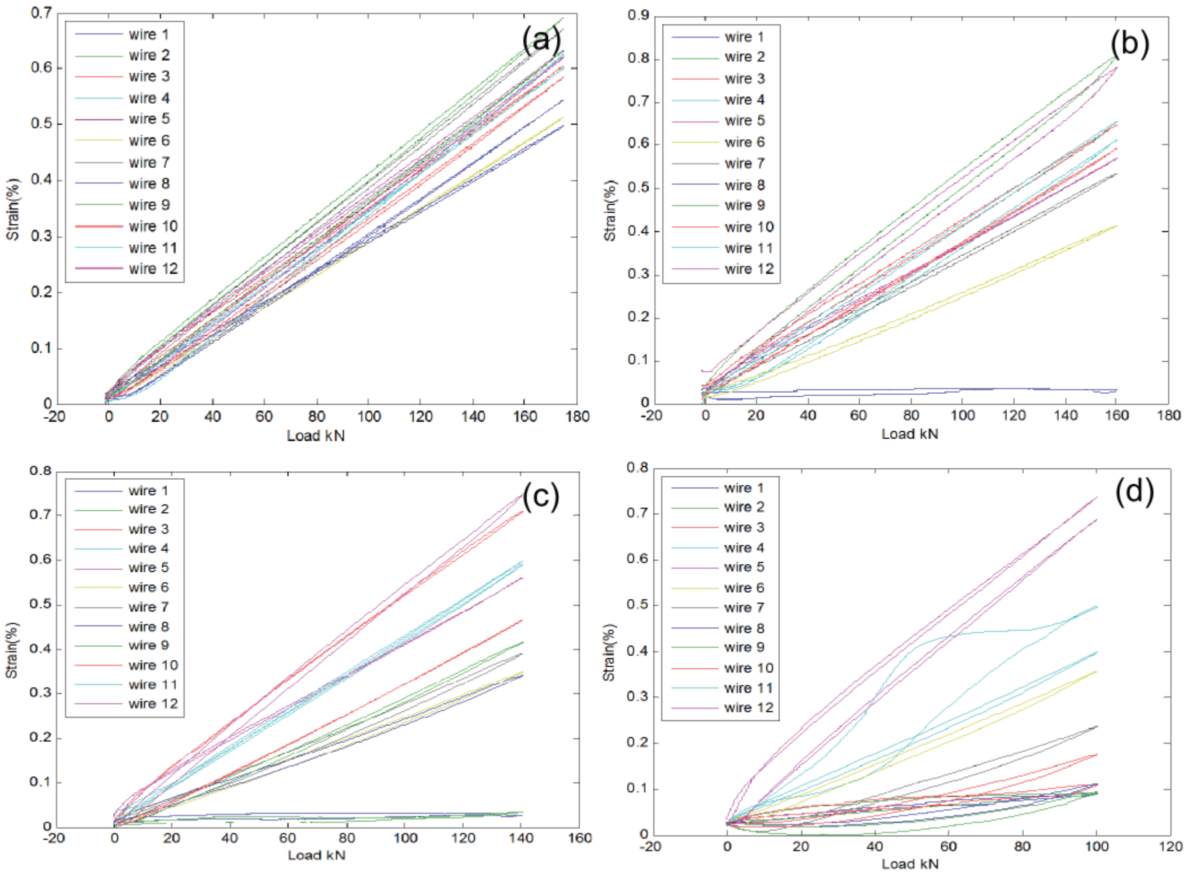

Figure 16: Strain-Load behaviour of the rope for four states: (a) Undamaged (b) Wire 1 broken (c) Wires 1 and 2 broken and (d) Wires 1, 2, 3 and 4 broken.

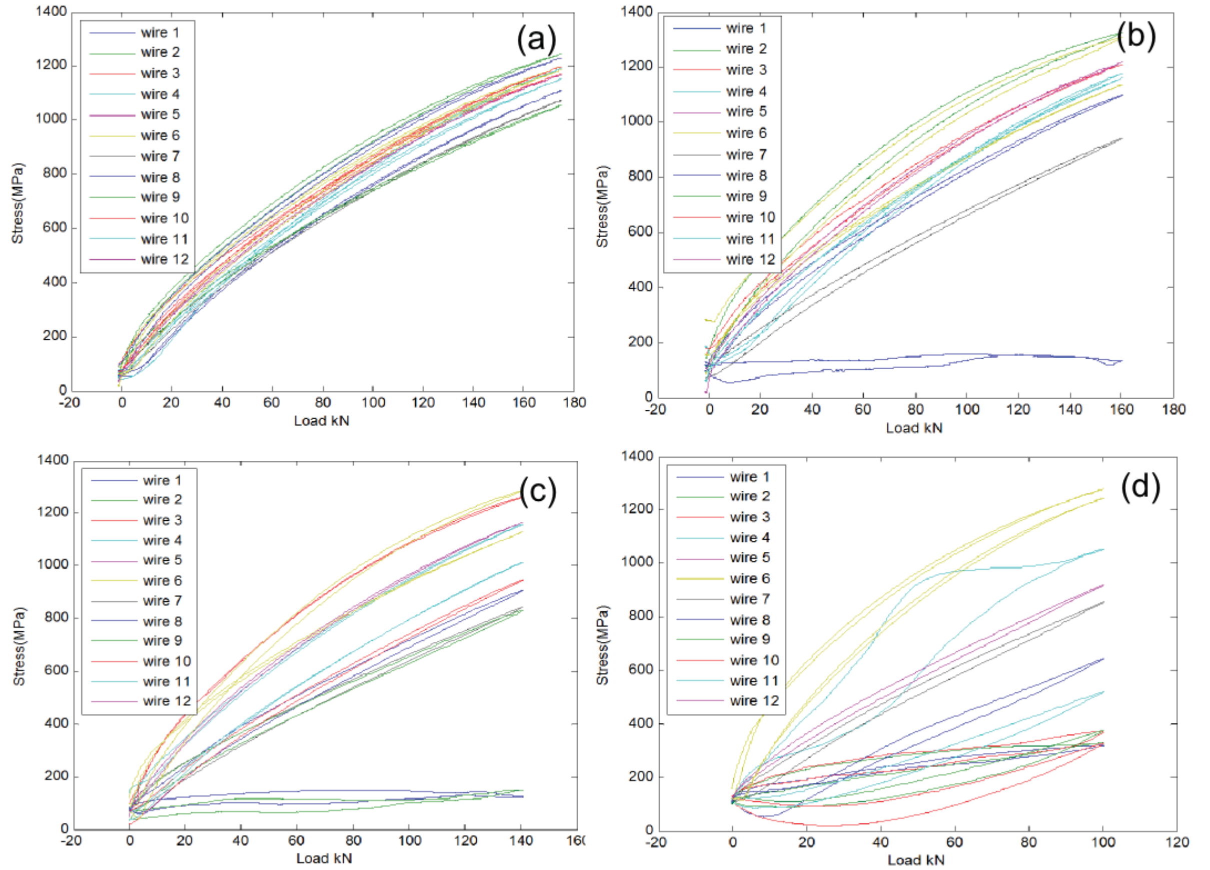

Figure 17: Stress-Load behaviour of the rope as derived from the non linear stress-strain behaviour for four states: (a) Undamaged (b) Wire 1 broken (c) Wires 1 and 2 broken and (d) Wires 1, 2, 3 and 4 broken.

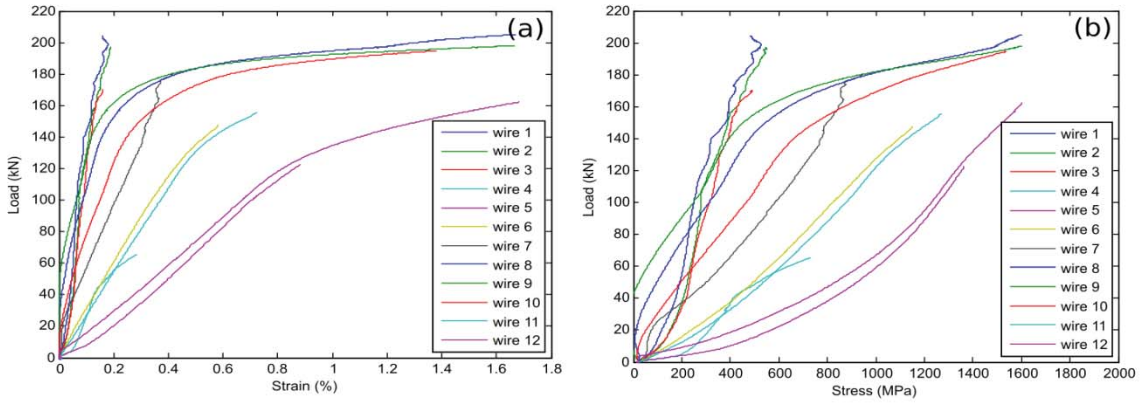

Figure 18: (a) Load-Strain and (b) Load-Stress behaviour for the rope with 4 wires broken taken up to breaking load.

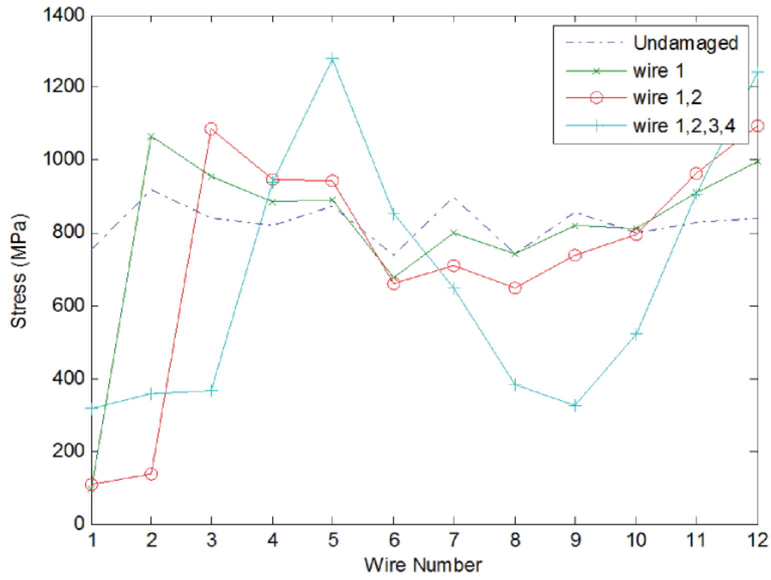

Figure 19: Stress in the wires for the 4 states at 100 kN load showing that the wires adjacent to the breaks taking more stress than the wires on the opposite sides.

9.3.1 Load sharing in the rope

By analysing these results in a slightly different way it also possible to obtain some insight into the load sharing of the external wires in the rope for different rope loads and infer the load taken by the internal wires. By calculating the load in the wire from the strain gauge measurement (by calculating stress and then multiplying by area) and dividing this by the load share assuming it is evenly distributed (i.e. rope load/number of wires), the load share is calculated. I.e the following relationship:

Load share (%) = 100 × Wire Stress / (L × N)

Where L is the rope load and N is the number of wires in the rope (19). Applying this relationship gives the percentage of load the wire is taking compared to that for a perfect rope: 100% would be the ideal value, above this means that the wire is taking more than its share and a lower value implies less. If these values are averaged between all twelve external wires then this provides an indication of how close the whole layer is to the ideal state.

Each test is plotted for a range of rope loads and these are shown in Figure 20 and Figure 21. What seems to be clear from this is that for this construction the external wires take significantly above their ideal share of load at low rope loads and this gradually drops to towards the ideal 100% value with increasing load. The implication of this is that the internal wires are taking very little (or possibly no load at all) at low rope loads and gradually take up load as the load in the rope increases. It seems that there may even be some compression in the internal wires at the very low loads since in theory if the external layer takes 160% of the load this should be the total rope load (i.e. because 19/12 = 160%). The mechanism of this load transfer on to the internal wires is not known but it may be through a gripping effect as the external layers squeeze down on the internal ones at higher loads, the phenomenon would require further investigation to fully characterize and understand it.

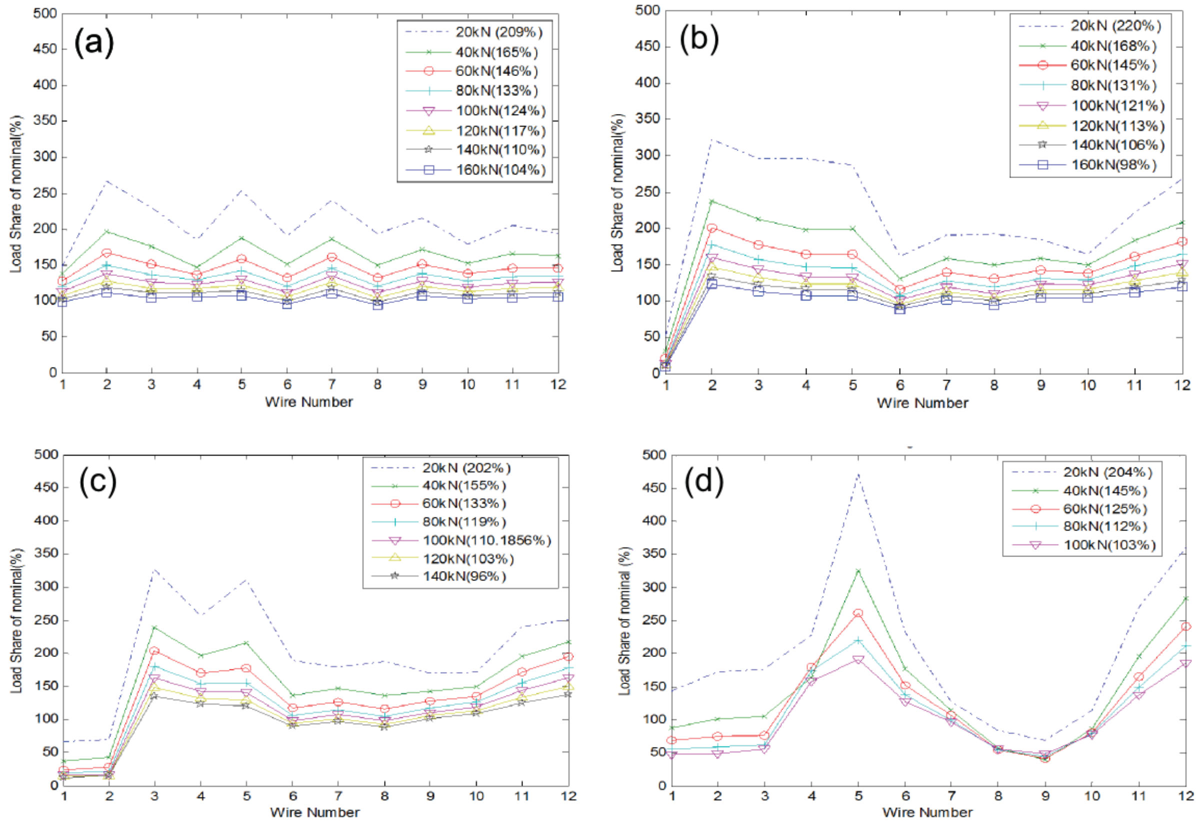

Figure 20: Load share in the wires for a range of rope loads for four states: (a) Undamaged (b) Wire 1 broken (c) Wires 1 and 2 broken and (d) Wire 1, 2, 3 and 4 broken.

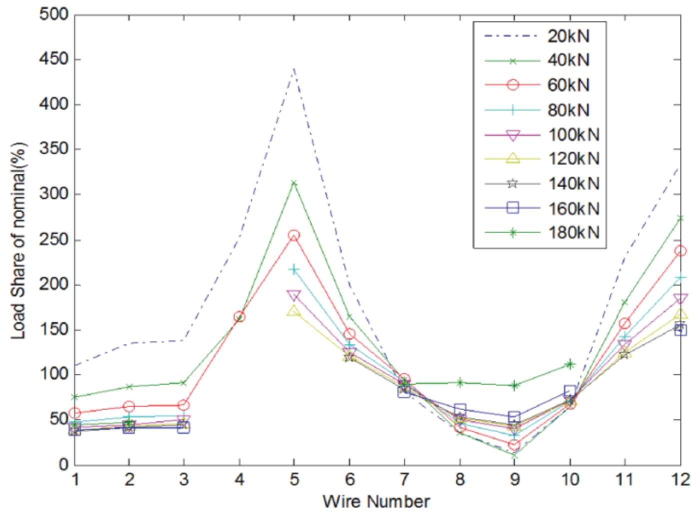

Figure 21: Load share in the rope with 4 wires broken for a range of loads, taken up to break load.

9.3.2 Comparison with calculations

The measured breaking strength of the spiral strand with 4 cut wires was 207 kN whereas the calculated breaking load was 170 kN.

Note that all the gauges failed before failure of the rope (Figure 22). On Figure 22 the behaviour of wires 12 and 8 has been extrapolated (dotted lines).

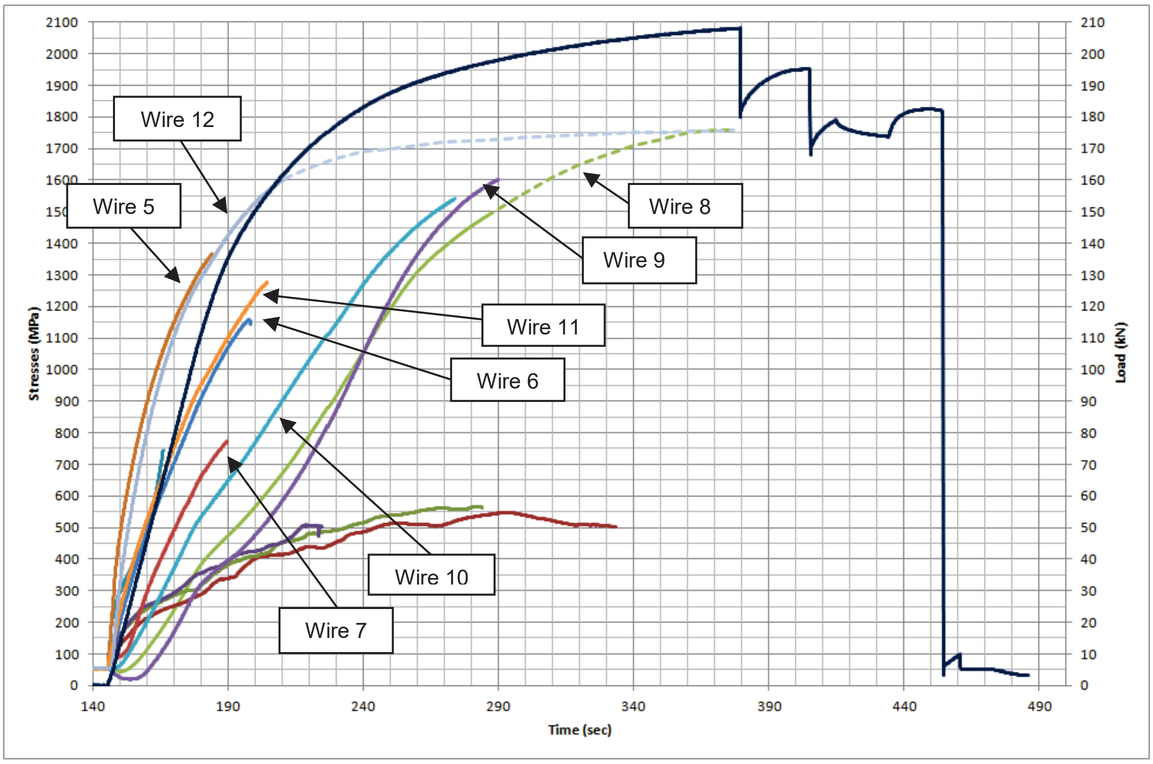

Figure 22: Breaking test – Stress versus time.

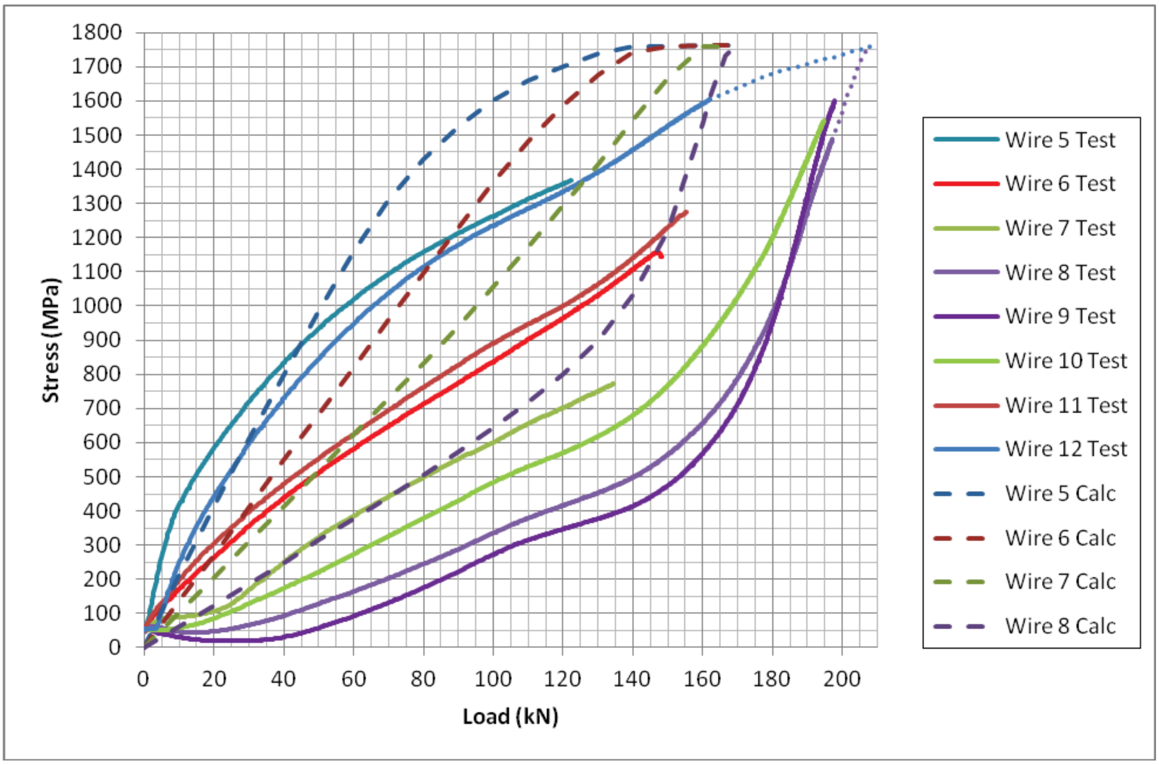

Figure 23: Comparison between calculations and test results.

The calculations are based on the maximum local stress, whereas the measurements with the strain gauges take into consideration the average stress in the area of the gauge.

Furthermore, the shape of the calculated wire is not round, and thus there is a kind of notch effect on the edge of the modelled wire which does not exist in reality.

The Figure 24 shows the results of the calculation for the wire 11. A difference of 100 MPa may be seen on the same section.

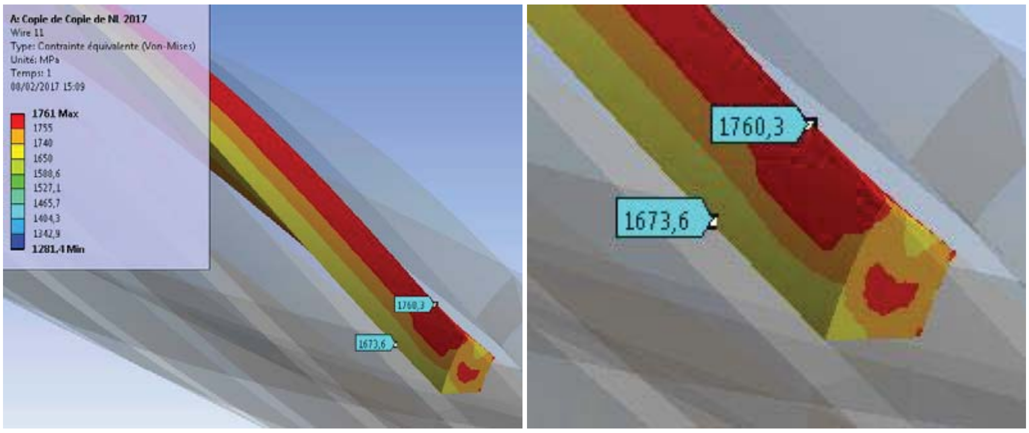

Figure 24: Stress distribution in the 3D model of the wire.

If it is assumed that the actual average stress is 100 MPa lower than the calculated one, the same stress will in fact be reached for a higher load than the one shown on the diagram (Figure 23).

For the most loaded wires (n°5 and n°6) a variation of the stress of 100 MPa in the flattened zone of the graph leads to a reduction of the load of about 40 kN (Figure 23).

Thus the corrected calculated breaking strength would be 170 + 40 = 210 kN, which is very close to the 207 kN that was measured.

So it may be said that the results of the calculations are in accordance with the results of the measurements.

10 Breaking tests with spiral strand ropes

10.1 Test results

The results of the testing with cut wires performed on the 1 × 19 and 1 × 37 spiral strand samples are presented in Tables 11 and 12.

Cut wires	%CSA cut	Comments	Breaking Load	% CSA residual	% residual strength	k
[-]	[%]	[-]	[kN]	[%]	[%]	[-]
0	0.0	no cut wires	260.0	100.0	100.0	1.000
2	10.4	2 symmetrical cut wires	232.2	89.6	89.3	1.029
4	20.9	4 symmetrical cut wires (2+2)	207.0	79.1	79.6	0.976
8	41.7	8 symmetrical cut wires (4+4)	153.7	58.3	59.1	0.981
1	5.2	1 cut wire	246.1	94.8	94.7	1.019
2	10.4	2 adjacent cut wires	222.4	89.6	85.5	1.394
4	20.9	4 adjacent cut wires	208.4	79.1	80.2	0.947
4	20.9	4 adjacent cut wires (10.7 m sample)	193.2	79.1	74.3	1.230
8	41.7	8 adjacent cut wires	154.7	58.3	59.5	0.971
8	41.7	8 adjacent cut wires (10.7 m sample)	152.6	58.3	58.7	0.990

Table 11: Cut wire tests on 1 × 19 spiral strand.

Cut wires	%CSA cut	Comments	Breaking Load	% CSA residual	% residual strength	k
[-]	[%]	[-]	[kN]	[%]	[%]	[-]
0	0.0	no wire breaks	285.7	100.0	100.0	1.000
2	5.4	2 adjacent cut wires	271.0	94.6	94.9	0.944
7	18.9	7 adjacent cut wires	230.3	81.1	80.6	1.026
7	18.9	4 on outer layer, 3 on second layer	218.9	81.1	76.6	1.238

Table 12: Cut wire tests on 1 × 37 spiral strand.

10.2 Analysis and comparison with calculations

Table 13 summarises the k factor for the different wire break configurations for the tests and computer model.

The results of the calculations (Table 9) and the tests (Table 11) agree for the symmetric configuration where the k factor is always close to 1.

However we notice significant differences for the asymmetric configurations where the measured breaking strength is bigger than the one calculated and the measured **k** factor remains close to 1, and quite often smaller than 1.

This can be partially explained by the high level of plasticity in the wires before failure revealed by the wire test. When this non linear behaviour is then incorporated into the model it allows more load sharing to take place before ultimate failure of the rope. It must also be considered that the wires within the sample can perform some geometrical adjustment, especially in the plasticity zone. The slow loading rate of the machine actuator will allow the rope to implement some geometrical change as the load increases.

This can also be partially explained by the fact that for the stranded ropes, each strand is more constrained by the others around it and is much less able to adjust. The k factors are thus significantly higher than those measured during the tests of the spiral strand ropes.

<table>
<tr><th>%CSA cut</th><th>Comments</th><th>Tests</th><th>Calculations bi-linear</th><th>Calculations non-linear</th></tr>
<tr><td></td><td></td><td>(Table 11)</td><td>(Table 9)</td><td>(Table 10)</td></tr>
<tr><td>[%]</td><td>[-]</td><td>[-]</td><td>[-]</td><td>[-]</td></tr>
<tr><td>10.4</td><td>2 symmetrical cut wires</td><td>1.03</td><td>0.95</td><td></td></tr>
<tr><td>20.9</td><td>4 symmetrical cut wires (2+2)</td><td>0.98</td><td>0.96</td><td></td></tr>
<tr><td>41.7</td><td>8 symmetrical cut wires (4+4)</td><td>0.98</td><td>1.01</td><td></td></tr>
<tr><td>5.2</td><td>1 cut wire</td><td>1.02</td><td>1.92</td><td></td></tr>
<tr><td>10.4</td><td>2 adjacent cut wires</td><td>1.39</td><td>1.92</td><td></td></tr>
<tr><td>20.9</td><td>4 adjacent cut wires</td><td>0.95</td><td rowspan="2">1.63</td><td rowspan="2">1.53</td></tr>
<tr><td>20.9</td><td>4 adjacent cut wires (10.7 m sample)</td><td>1.23</td></tr>
<tr><td>41.7</td><td>8 adjacent cut wires</td><td>0.97</td><td rowspan="2">1.34</td><td></td></tr>
<tr><td>41.7</td><td>8 adjacent cut wires (10.7 m sample)</td><td>0.99</td><td></td></tr>
</table>

Table 13: Comparison of the k factor between tests and calculations.

It appears then that the k factor is not a relevant parameter for spiral strands and a k factor close to 1, or even smaller than 1 does not mean that there is no load imbalance at lower loads as we have demonstrated with the modelling (Figure 13, Table 10), and with the gauge results (Figures 20 and 21 - very clearly showing that the load share gradually becomes more even as the load increases). In order to distinguish this phenomenon from the k factor we have called this the amplification factor which is calculated on the basis of the stress in the wire at a given rope load (Table 10). It was also noted that at the low loads the external wire layer appears to take more than its share of load but that the value tends towards the ideal value as the load increases.

Although, the k factor is not a relevant parameter for identifying the working conditions of a spiral strand, it is noted that, the k factor does have some sensitivity to the degree of asymmetry (Figure 25, Table 12).

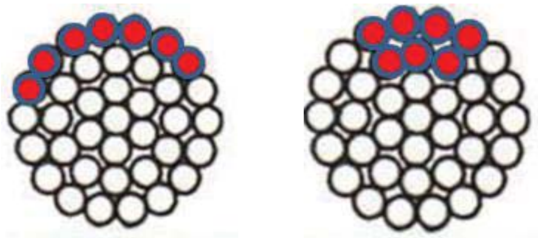

(a) (b)

Figure 25: For the same loss of metallic area (A/A_0=81.1%), the remaining strength is 230.3 kN (k = 1.03) for the configuration (a) whereas it is only 218.9 kN (k = 1.24) for the configuration (b).

11 Conclusions

In the case of a stranded rope the distribution of the wire breaks has a significant impact on the breaking strength of the rope. If the broken wires are localized in the same zone of one strand, the k factor can be assumed to be at least 3 for a loss of metallic area of 5% and if distributed on two strands, the k factor can be assumed to be at least 2 for a loss of metallic area of 10%.

This should influence the counting of the broken wires for the determination of the discard criteria.

For the spiral strand ropes however, the loss of strength seems to consistently match the loss of area independent of the level of asymmetry in the wire break configuration (i.e. k remains close to 1 for all cases).

This does not mean that there is not a large imbalance of loads in the wires for asymmetric breaks however and we have clearly demonstrated this through the strain gauge results. The point is that before the ultimate failure of the strand some kind of evening out processes takes place and so the imbalance is not reflected in the k value.

In order to reflect this behaviour, it is proposed that another factor is used to account for this which is termed the amplification factor (see definition just above Table 10).

It must be taken into account that this amplification is bigger for a rope in operation (safety factor 5 to 3), than for a rope loaded close to its breaking strength.

An amplification factor of at least 2 seems appropriate for the configuration with 4 cut wires.

So the assessment of the remaining capability of the rope shown in Figure 1, which depends on the actual safety factor for a given load, should be performed on the basis of an amplification factor of at least two, thus without taking into account the external layer of wires.

12 Acknowledgements

The authors would like to thank Mr. Barry Winfield and Mr. Robert Carr both of TTI Testing, Wallingford for preparing the many wire rope samples which were broken during the course of this work.

Thanks are also due to Prof. Roger Hobbs who read through various drafts of this paper and made many helpful suggestions for improvements.

13 References

[1] Oplatka, G. and Roth, M. Relation between number and distribution of wire breaks and the residual breaking force, Proceedings of the OIPEEC Conference 'Wire Rope Discard Criteria', Zurich, Switzerland, 6th - 9th September 1989,.

[2] Borello, M., Kuun, T.C, Wainwright, E.J, James, A. and Hecker, G.F.K. The Safe use of Mine Winding Ropes, Volume 4: Studies towards a Code of Practice for Rope Condition Assessment, Published by Safety in Mines Research Advisory Committee (SIMRAC), Project GAP 054, April 1996.

[3] Ridge, I.M.L., Teissier, J.M. and Verreet, R. *The effect of wire rope “safety” clamps on rope terminations*, Proceedings of the OIPEEC Conference "Simulating Rope Applications" (ed. I.M.L. Ridge) Oxford, UK 10th-12th March 2013, 17-32 ODN 0892 ISBN: 978-0-9552500-4-0.

[4] Evans, J.J., Ridge, I.M.L. and Chaplin, C.R. ‘Wire strain variations in normal and overloaded ropes In Tension-Tension fatigue conditions and their effect on endurance’ - Journal of Strain Analysis 2001 36(2) pp219-230.